Chemical Engineering Journal 519 (2025) 164794

Contents lists available at ScienceDirect

Chemical Engineering Journal

journal homepage: www.elsevier.com/locate/cej

Synergistic transition multi-metal coatings drive sub-melting-point reaction of aluminum

Lei Yang [1], Yuxin Zhou [1], Mahbub Chowdhury, Yuan Qin, Matthew M. Dickson, Michael R. Zachariah [*]

Department of Chemical and Environmental Engineering, University of California, Riverside, CA 92521, United States

ARTICLE INFO

Keywords:
Aluminum nanoparticles
Eutectic melting
Alloying reactions
Nanothermite ignition

ABSTRACT

Aluminum (Al) nanoparticles are high-energy additives for propellants and explosives, yet their performance is constrained by the native alumina shell and particle coalescence. To overcome this limitation, we introduce a synergistic transition metal coating strategy using cobalt (Co), nickel (Ni), and copper (Cu). A one-pot, scalable synthesis method was developed to fabricate Al@CoNiCu nanoparticles, where exothermic Al-Ni/Co intermetallic reactions and low-temperature Al-Cu eutectic melting act in concert. This dual mechanism triggers outward flow of molten Al, well below the melting point of pure Al, creating a self-sustaining ignition feedback loop. *In situ* transmission electron microscopy (TEM) directly captures the formation of nanocracks and subsequent Al outflow, which exposes the reactive core to oxidizers, accelerating ignition. Gibbs free energy of the alloying processes indicates that Al@CoNiCu ($\Delta G \sim -24.7$ kJ·mol^{-1}) has the highest tendency to form mixed alloy and is mainly driven by the high exothermicity of the Al–Co/Ni reactions (-20.1 kJ·mol^{-1}) and the favorable entropy of mixing ($T\Delta S_{mix} \sim 4.6$ kJ·mol^{-1} at 870 K). By tuning the Co/Ni/Cu coating, we achieve precise control over ignition temperatures, offering a versatile approach to tailor nanothermite reactivity.

1. Introduction

The integration of nanostructures into energetic materials has spurred a surge in research aimed at developing high-performance, next-generation fuel systems [1–5]. Aluminum (Al) particles, above all metals, are pivotal additives in propellants and explosives due to their exceptional energy density, abundance, and low cost [1,6]. However, the full potential of Al additives remains hindered by intrinsic challenges [7–9]. The native alumina shell on Al particles forms a stable, compact barrier that protects the underlying Al from interacting with oxidizers often prematurely, until either Al diffuses out through the alumina shell [10], or when the Al core melts, creating nanocracks through volume expansion and exposing fresh Al to the environment [11]. Although reducing particle size from micron to nanoscale can lower the ignition threshold due to the increased surface area and decreased diffusion distance [11], further reduction of the ignition temperature is limited by the melting point of Al (~933 K) and the tendency of molten particles to coalesce, leading to combustion rates that fall short of the theoretical predictions [7,8].

Transition metal coatings on micron-sized Al particles have recently demonstrated superior combustion properties compared to conventional Al-doped fuels [12–15]. For instance, nickel (Ni) and cobalt (Co) coatings can trigger highly exothermic intermetallic reactions with Al, generating significant heat that promotes the melt dispersion of the Al core and accelerates ignition [12–14]. Previous studies on micron-sized Al@Ni and Al@Co particles have shown that Al@Ni-based propellants exhibit higher regression rates, while Al@Co systems display improved energy release, partly due to the catalytic effect of Co [14]. However, as the eutectic melting point of Al-Ni (~910 K) and Al-Co (~930 K) [16,17] are close to that of pure Al, these coatings do not effectively lower the melting point of the Al core, thus limiting the further reduction of the ignition temperature.

In contrast, copper (Cu) coatings offer a unique advantage due to the low eutectic melting temperature of the Al-Cu system [18,19]. Zhou et al. [20] in developing core-shell structured phase change material for thermal storage, demonstrated that depositing Cu onto Al microparticles via replacement reactions resulted in a tunable suppression of melting points between 820 and 865 K, significantly lower than those of pure Al

* Corresponding author.
E-mail address: mrz@engr.ucr.edu (M.R. Zachariah).
[1] Co-first authors contributed equally to this work.

https://doi.org/10.1016/j.cej.2025.164794
Received 1 April 2025; Received in revised form 30 May 2025; Accepted 11 June 2025
Available online 13 June 2025

(933 K) and Cu (1356 K). Furthermore, Cu is among the fastest diffusing substances in alumina, with a diffusion coefficient (D) orders of magnitude higher than those of Ni and Co (at 1500 K, $D \sim 3.0 \times 10^{-12}$, 3.0×10^{-16}, and 9.8×10^{-17} $cm^2 \cdot s^{-1}$ in monocrystalline alumina for Cu, Ni, and Co, respectively) [21,22]. Recent *in situ* TEM studies by Xu et al. [23,24] provide additional insight: they prepared Al-Cu wire bonds by FIB thinning of as-bonded samples and performed isothermal annealing below 500 K. Their observations revealed that Cu diffuses rapidly through fragmented and defect-rich regions of the native ~5 nm alumina layer after ultrasonication via fracture-induced pathways such as grain boundaries and dislocations [25], with a relatively low activation energy of ~61 kJ/mol for Al_2Cu nucleation [23–25]. Defect-assisted diffusion is significantly faster than bulk lattice diffusion due to the reduced energy barriers along imperfections [21,26], allowing the rapid migration of Cu through the alumina barrier and the formation of intermetallic compounds (Al_2Cu, Al_4Cu_9) at relatively low temperatures. Therefore, coating Al nanoparticles with Cu can induce early intermetallic formation, which lowers the local eutectic melting point and generates localized mechanical stress that promotes nanocrack formation in the alumina shell, ultimately accelerating ignition.

Most previous studies on Al@Ni and Al@Co have focused on Al micron-sized particles because coating metals onto Al nanoparticles presents significant challenges [12,14,15]. Traditional coating methods, such as replacement reactions [12,14,15], require the removal of the native alumina shell, thereby exposing the highly reactive Al core, which is extremely prone to oxidation at the nanoscale. Moreover, research on Al@Cu remains limited [20], with a notable lack of studies on its combustion properties and the underlying reaction mechanisms. A central unresolved question is whether the enhanced ignition and combustion performance of the Al particles coated with transition metal is primarily driven by diffusion of the coating metal (or Al) through the alumina shell, or by mechanical cracking of the shell due to thermal stresses.

This work focuses on the application and mechanism study of Al nanoparticles coated with various transition metals. We developed a one-pot and scalable synthesis method for $Al@Co_{0.146}$, $Al@Ni_{0.147}$, $Al@Cu_{0.076}$, and $Al@Co_{0.059}Ni_{0.056}Cu_{0.063}$ nanoparticles (hereafter abbreviated as Al@Co, Al@Ni, Al@Cu and Al@CoNiCu). In particular, Al@CoNiCu was rationally designed to combine the advantages of highly exothermic Al-Ni and Al-Co intermetallic reactions with the low eutectic melting characteristic of the Al-Cu system. Such transition-metal coatings have also been shown to help suppress agglomeration of molten Al during combustion by promoting early melt dispersion [12,27] and physically constraining the particle surface [12,20]. This synergistic approach enables nanocracking of the alumina shell and complete outward flow of molten Al at temperatures as low as ~837 K, thereby significantly reducing the ignition temperature. The underlying mechanisms were elucidated using thermogravimetric analysis/differential scanning calorimetry (TGA/DSC) and *in situ* transmission electron microscopy (TEM). By resolving the interplay between diffusion-driven intermetallic formation and mechanical cracking of the oxide shell, this study provides a unified framework for optimizing the combustion performance of transition metal-coated Al nanoparticles.

2. Experimental methods

2.1. Synthesis of transition-metal-coated Al nanoparticles

Al nanoparticles (US Research Nanomaterials, 100 nm) were coated with transition metals (Co, Ni, Cu) following a similar procedure. First, Al nanoparticles were dispersed by ultrasonic oscillation in a methanolic solution of metal salts, including $NiCl_2 \cdot 6H_2O$ (Alfa Aesar, 99.95 %), $CoCl_2 \cdot 6H_2O$ (Fisher Scientific, 98 %), and $CuCl_2 \cdot 2H_2O$ (Acros Organics, 99 %). Then a methanolic solution of excess NH_3BH_3 (Sigma-Aldrich, 90 %) was introduced to reduce metal ions onto the Al nanoparticle surfaces. The mixture was sealed and maintained in a 40 ± 2 °C water bath, with continuous ultrasonic oscillation for 80 min (Fisher Scientific ultrasonic heater FS30D, cooling water added every 20 min). Finally, the resulting particles were washed and cooled with methanol (to halt the nucleation of the transition metals and remove impurity), and then separated by centrifugation (10^4 rpm, 10 min). Details of the formulation are provided in Supplemental Table S1. Antistatic wrist traps and grounding mat were used during the handling of synthesized particles.

To quantify the elemental composition of these particles, we performed microwave-assisted acid digestion followed by inductively coupled plasma optical emission spectroscopy (ICP-OES). Each powdered sample (5 mg) was weighed into a Teflon digestion vessel and digested using a MiniWAVE microwave digestion module (SCP Science, 6 × 75 mL configuration). Each sample was treated with nitric acid (HNO_3, 70 %) and hydrochloric acid (HCl, 35 %). Vessels were sealed and heated in the microwave with 100 % power for 20 min with regulation point at 70 psi. After cooling, the digests were filtered and diluted with Millipore water for the following ICP-OES tests (PerkinElmer Optima 7300DV). Calibration standards were included to ensure analytical accuracy.

2.2. T-jump ignition and TOFMS

T-jump ignition techniques were used to measure the ignition temperature of Al@Co, Al@Ni, Al@Cu, and Al@CoNiCu during the thermite reactions. Details of techniques and the schematic setup can be found in Fig. S12 and our prior works [28–30]. Nascent Al, Al@Co, Al@Ni, Al@Cu, and Al@CoNiCu (3 mg) were mixed with CuO nanoparticles (US Research Nanomaterials, 70 nm) in hexane (1 mL) by ultrasonic oscillation. The equivalence ratio of 0.67 was used to pursue the complete oxidation of Al particles and their coatings. Then the mixtures were deposited on a Pt wire (~76 μm in diameter, ~1 cm in length). Since samples were handled in small quantities and dispersed in solution with only a few microliters drop-cast onto a 75 μm Pt wire, the actual mass per ignition was therefore well below 1 mg. A 3 ms high-voltage pulse was delivered to the wire, resulting in an ultra-fast heating rate of $\sim 10^5$ $K \cdot s^{-1}$. The temperature of the Pt wire was calculated from its electrical resistance. For ignition temperature measurements, the high-voltage pulse would simultaneously trigger a high-speed monochromatic camera (Vision Research Phantom V12.1) working at 67,000 fps to video the combustion events and record the ignition delay time. In TOFMS, the fuel and oxidizer nanoparticles were ignited in a high vacuum (10^{-7} Torr). Released gas-phase species were ionized by 70 eV electron beams, accelerated in a linear time-of-flight chamber, and detected by a microchannel plate. Time-resolved spectra were recorded using a digital Teledyne Lecroy oscilloscope.

2.3. TGA-DSC

TGA-DSC measurements were carried out using a NETZSCH STA 449 F3 Jupiter thermogravimetric analyzer, with a temperature ramp rate of 10 $K \cdot min^{-1}$ up to a final temperature of 1473 K, under an argon flow of 50 $mL \cdot min^{-1}$. Roughly 3 mg of sample was used for each run for safety reasons.

2.4. In situ STEM-EDS

In situ observations of nanoparticle dynamics and EDS analysis were performed using a scanning transmission electron microscope (FEI Titan Themis 300) equipped with an X-FEG electron gun operating at 200–300 kV in a vacuum chamber maintained at 10^{-7} Torr. The samples were sonicated in hexane for dispersion, then drop-casted onto the SiC heating membrane of Fusion AX E-chips (Protochips Inc.). These E-chips are subsequently assembled into the corresponding electrical TEM holder designed for *in situ* heating experiments, enabling simultaneous high-angle annular dark-field (HAADF) imaging and EDS elemental mapping. Temperature was precisely controlled and monitored by the

Fusion AX system, providing uniform heating at a rate of ~10 K·min^{-1} from room temperature up to 1470 K. Besides fast imaging on the whole heating process with TEM, EDS images were also collected after reaching each designated temperature (like 870 K) while holding each temperature stage for 1 min. This procedure allowed us to capture real-time dynamic changes in the nanoparticle structure under well-defined thermal conditions. The electron beam was kept blocked except for alignment and image acquisition to minimize electron gun effects on the particles.

3. Results and discussion

3.1. Characterization of coated Al nanoparticles

Al nanoparticles were coated with transition metals via a one-pot synthesis. Briefly, the Al nanoparticles were first suspended in methanol solutions containing $CoCl_2$, $NiCl_2$, and $CuCl_2$. Subsequently, NH_3BH_3 was added as a reductant to deposit Co, Ni, and Cu onto the native alumina shell of the Al nanoparticles (see Fig. 1(a) for a schematic illustration). The overall chemical reactions are in Eqs. (1)–(3). The detailed synthesis procedure is described in Section 2.1 and Supporting Table S1. As confirmed by TEM images and EDS mapping (Fig. 1(b)), the resulting Al@CoNiCu nanoparticles exhibit clear core-shell structures with amorphous Co, Ni, and Cu coatings (average thickness ~ 13 nm from TEM-EDS line scans). Size distributions of the synthesized particles under SEM are shown in supporting Fig. S1, with an average diameter of ~100 nm. The relative mole fraction of Al: Co: Ni: Cu is ~1: 0.059: 0.056: 0.063 in the synthesized Al@CoNiCu nanoparticles and 1: 0.146, 1: 0.147, 1: 0.076 for Al@Co, Al@Ni, Al@Cu, respectively, determined from ICP-OES after microwave digestion. Chemical compositions of the synthesized particles are detailed in Supporting Table S2. The core-shell TEM for Al@Co, Al@Ni, and Al@Cu are in Figs. S5(a)–S7(a). In previous works on micron-sized Al@Ni, Zhang et al. [12] used 200-nm Ni coating for 13-um Al@Ni; while Wang et al. [13] used 400-nm Ni and 200-nm P dual-layer coating for 15-um Al@Ni-P. Although transition metal coatings can enhance ignition properties, they may also reduce the active Al content due to the added mass of the coating, particularly in nanoparticles with high surface area-to-volume ratios. Therefore, the

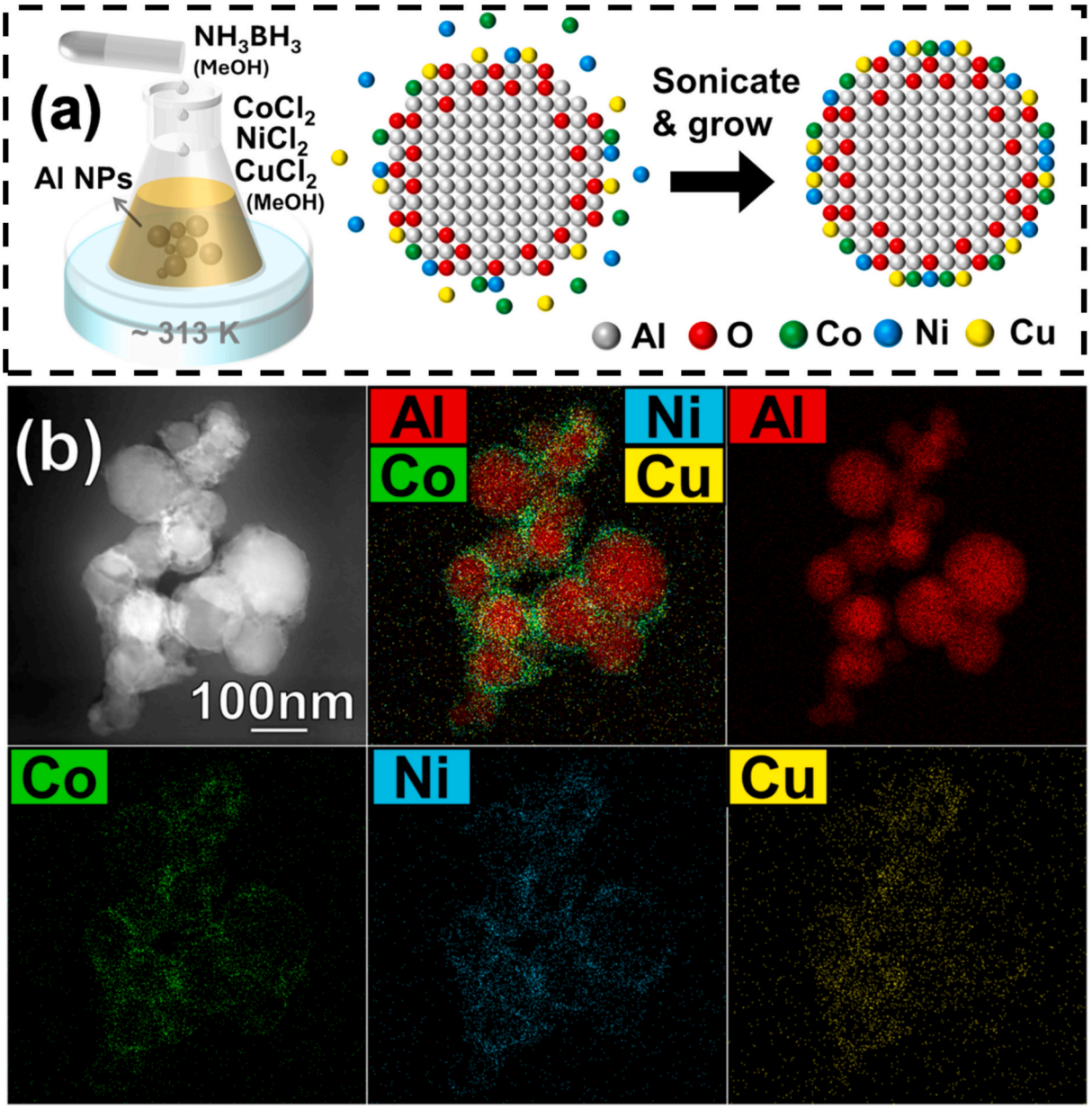

Fig. 1. (a) Synthesis method of Al@CoNiCu nanoparticles, and (b) their core-shell structures imaged in TEM-EDS.

optimized coating quality, Al@$Co_{0.146}$, Al@$Ni_{0.147}$, Al@$Cu_{0.076}$, and Al@$Co_{0.059}Ni_{0.056}Cu_{0.063}$, is crucial to balance improved ignition performance with the retention of active Al content.

$$2CoCl_2 + NH_3BH_3 = 2Co\ (s) + NH_4BCl_4 + H_2\ (g) \quad (1)$$

$$2NiCl_2 + NH_3BH_3 = 2Ni\ (s) + NH_4BCl_4 + H_2\ (g) \quad (2)$$

$$2CuCl_2 + NH_3BH_3 = 2Cu\ (s) + NH_4BCl_4 + H_2\ (g) \quad (3)$$

3.2. T-jump ignition and TOFMS characterization

Table 1 summarizes the T-jump ignition temperature of Al@Co, Al@Ni, Al@Cu, and Al@CoNiCu measured either in air (1 atm), or when mixed with CuO nanoparticles in an argon environment for nanothermites applications. Details of the T-jump ignition with the high-speed camera and TOFMS techniques can be found in Section 2.2 and our prior works [28–30]. In air, the nascent Al powder does not ignite during the rapid T-jump from 300 K to 1500 K within 3 ms due to sintering, consistent with our previous studies [31–33]. In contrast, ignition of the coated particles are substantially lower in air: ~910 K for Al@Co, ~900 K for Al@Ni, and ~960 K for Al@Cu. Most notably, the Al@CoNiCu nanoparticles exhibit the lowest ignition temperature at ~840 K in air, roughly 100 K lower than the melting point of pure Al.

For the Al@X + CuO nanothermites (X = Co, Ni, Cu, or CoNiCu), an equivalence ratio (φ) of 0.67 was used to ensure excess CuO. The ignition temperatures of the Al@Co + CuO nanothermite (~930 K) and Al@Ni + CuO (~950 K) show apparent improvements over the nascent Al + CuO nanothermites (~1180 K); The Al@Cu + CuO nanothermite (~1110 K) also shows a reduction of ~70 K. These differences stem from the varying amounts of heat released by different intermetallic reactions, a topic further explored in Section 3.3. Although optimization of the weight percentage and coating thickness for Al@Co and Al@Ni suggests inherent difficulty in lowering their ignition temperatures below the Al melting point, the Al@CoNiCu particles achieve a dramatic decrease to ~860 K, approximately 70 K below pure Al's melting point. Moreover, the average ignition time for Al@CoNiCu is the shortest (~1.5 ms) compared to Al@Co (~1.7 ms), Al@Ni (~1.8 ms), and Al@Cu (~2.3 ms) in the T-jump experiments.

Fig. 2(a–b) shows representative mass spectra from the T-jump ignition of the Al@CoNiCu + CuO sample, compared with background spectra under vacuum conditions (10^{-6} Torr). The background signal (m/z = 17, 18, and 28) arises from the electron impact ionization of H_2O and N_2. Upon rapid T-jump heating of the nanothermite to ~1250 K within 3 ms, signals from O, Al, and O_2 (m/z = 16, 27, and 32) were observed. The O_2 signals from CuO decomposition ($4CuO \rightarrow 2Cu_2O + O_2$) [29] can serve as an indicator for the onset temperature of the thermite reaction ($2Al + 3CuO \rightarrow Al_2O_3 + 3Cu$), which accelerates the O_2 release through fast heat generation. As shown in Fig. 2(c–h), the onset temperature of O_2 release for Al + CuO (1100 K) is close to that of pure CuO (1120 K), indicating that O_2 release from CuO decomposition is a critical step in the thermite reaction, aligning with our previous works [29,34]. In comparison, the O_2 onset of Al@Co + CuO (990 K) and Al@Ni + CuO (960 K) are lower than Al@Cu + CuO (1070 K), consistent with their ignition temperatures. In contrast, the O_2 release temperature of Al@CoNiCu + CuO is further reduced to 860 K, indicating that the thermite reaction initiates well below the melting point of bulk Al.

Table 1
Ignition and O_2 release temperatures of nascent Al, Al@Co, Al@Ni, Al@Cu, and Al@CoNiCu in the T-jump experiments using different oxidizers (heating rate ~ 10^5 K·s^{-1}).

Al@X	Al@X in air (1 atm)	Al@X + CuO (φ ≈ 0.67) in argon	
	Ignition temperature (K)	Ignition temperature (K)	O_2 release temperature (K)
Nascent Al	>1500	1180 ± 30	1100
Al@Co	910 ± 30	930 ± 30	990
Al@Ni	900 ± 30	950 ± 40	960
Al@Cu	960 ± 10	1110 ± 10	1070
Al@CoNiCu	840 ± 10	860 ± 30	860
CuO			1120

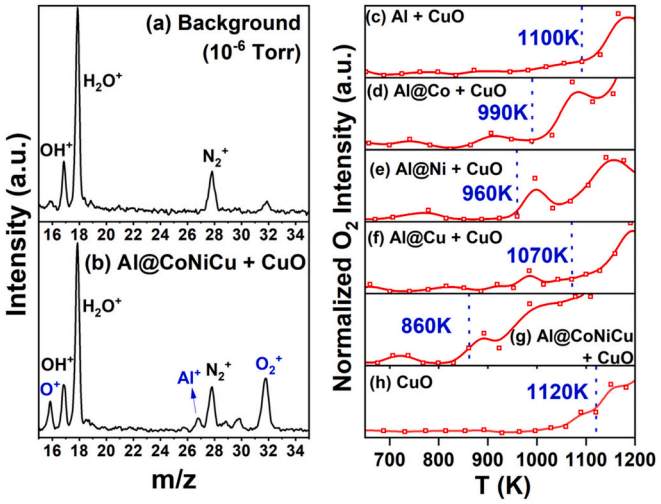

Fig. 2. Representative T-jump mass spectra of (a) background (10^{-6} Torr) and (b) Al@CoNiCu + CuO; Intensity of the O_2 release signal in (c) nascent Al, (d) Al@Co, (e) Al@Ni, (f) Al@Cu, and (g) Al@CoNiCu with CuO (φ = 0.67) in comparison with (h) pure CuO in T-jump mass spectrometry (heating rate ~ 10^5 K·s^{-1}).

3.3. Differential scanning calorimetry (DSC) and thermochemistry

Fig. 3 presents the DSC analysis of nascent Al, Al@Co, Al@Ni, Al@Cu, Al@CoNiCu, and Al_2O_3 nanoparticles with the hybrid metal coating (Al_2O_3@CoNiCu) for comparison. All TGA-DSC measurements were performed in an argon atmosphere with a heating rate of 10 K·min^{-1}, as detailed in Section 2.3. As sample masses remain nearly constant during heating in argon, we focus solely on the thermal events. For Al@Co, the DSC curve displays an exothermic peak at ~770 K, attributed to the Al-Co intermetallic reaction, followed by an endothermic peak at ~930 K, which corresponds to the eutectic melting of Al-Co (930 K) [35,36], or the melting temperature of pure Al (933 K). In Al@Ni, a series of continuous exothermic peaks were observed from 740 to 900 K, reflecting progressive Al-Ni alloying reactions, with the subsequent eutectic melting of Al-Ni at 910 K. No separate melting peak near 930 K was detected for Al@Ni, indicating that Al core completely melted due to Al-Ni eutectic reaction. In contrast, Al@Cu exhibits only a subtle exothermic peak at 750–800 K when heated at 10 K·min^{-1} (this signal becomes more pronounced at a slower heating rate of 1 K·min^{-1} as shown in Supplemental Fig. S2). The endothermic melting peak of Al@Cu at ~840 K is much earlier than those of Al@Co and Al@Ni, highlighting the low eutectic melting of Al-Cu (see Figs. S8–S10) [18,19]. Notably, Al@CoNiCu nanoparticles display two distinct exothermic events: one in the 700–750 K range, associated with the Al-diffusion-induced intermetallic formation; and another between 800 and 900 K, corresponding to Al-outflow-induced intermetallic reactions. The cumulative heat release is so significant that no separate endothermic melting peaks are detected above 910 K, implying complete alloying of Al below 900 K, which is further confirmed by subsequent TEM observations in Section 3.4. In comparison, the DSC curve of Al_2O_3@CoNiCu displays no exothermic or endothermic peaks, confirming that the alloying among Co, Ni, and Cu are nearly thermoneutral, and the amorphous-to-crystalline transition of the coating has negligible contributions; hence, the intermetallic reactions involving Al with Ni and Co are the primary contributors of exothermic heat in

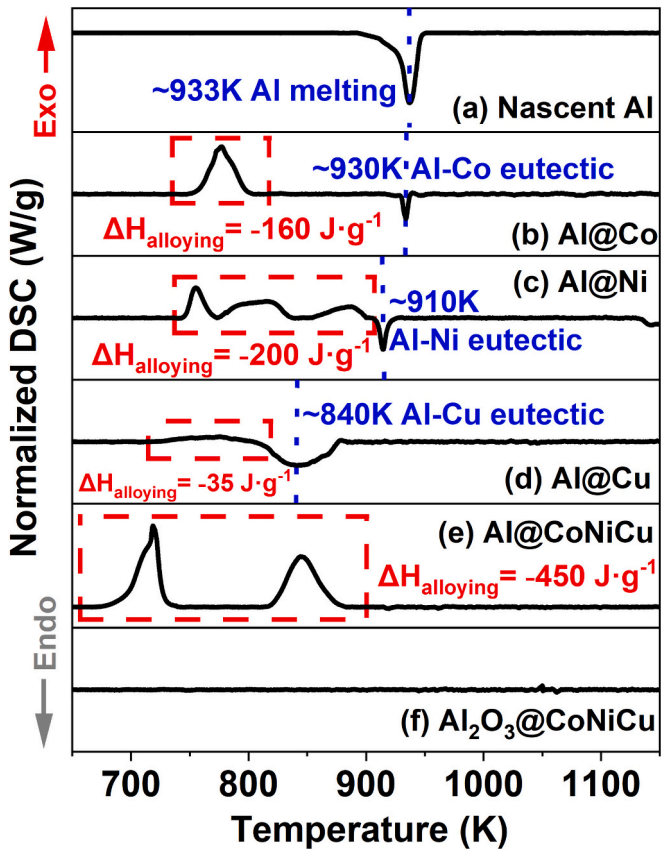

Fig. 3. DSC curves of (a) Al, (b) Al@Co, (c) Al@Ni, (d) Al@Cu, (e) Al@CoNiCu, and (f) Al_2O_3@CoNiCu in argon environment (heating rate 10 K·min^{-1}), and corresponding heat release per gram sample.

Al@CoNiCu.

Table 2 compiles the enthalpies of key thermochemical processes during heating of Al@X samples (assuming 1 mol Al), as extracted from phase diagrams and literature data. A comparison between Fig. 3 with Table 2 provides a comprehensive understanding of the thermochemical events in each sample. Assuming that direct alloying on the Al surface enables rapid heat transfer throughout the entire particle, the heat released in Al@Co (−160 J·g^{-1}), Al@Ni (−200 J·g^{-1}), and Al@CoNiCu (−450 J·g^{-1}) is sufficient to raise the particle temperature by >150 K (given that Al heat capacity is 0.9 J·g^{-1}·K^{-1}). Notably, only Al@CoNiCu releases enough heat to overcome the enthalpy of fusion (+390 J·g^{-1}) required for complete Al melting. As detailed in Table S3, in the $Al@Co_{0.146}$ and $Al@Ni_{0.147}$ samples, only ~30 % of the coated Co and Ni react with Al, causing their exothermic alloying reactions to appear as separate peaks from the subsequent endothermic melting event observed in DSC. In contrast, in $Al@Co_{0.059}Ni_{0.056}Cu_{0.063}$, nearly all the coated metals react with Al, and the extensive heat release causes the melting event to overlap with the exothermic peaks. Specifically, the highly exothermic reactions of Al + Ni (−68 kJ·mol^{-1}) and Al + Co (−35 kJ·mol^{-1}) are the major contributors to heat release in Al@CoNiCu; whereas in Al@Cu, the mildly exothermic reaction of Al + Cu overlaps with the endothermic eutectic melting of Al-Cu, resulting in a delayed and broadened melting event in DSC. This detailed thermal analysis underscores how the interplay between diffusion-controlled intermetallic formation and melting behavior governs the ignition characteristics of transition metal–coated Al nanoparticles.

Table 2
Thermochemical processes involved in the heating processes of Al nanoparticles coated with transition metals (enthalpies corresponding to 1 mol Al).

Events and temperature		Thermochemical processes	ΔH° (kJ·mol^{-1})
Al alloying reactions	700–900 K	Al (s) + 2/9 Co (s) → 1/9 Al_9Co_2 (s)	−35 [37]
		Al (s) + 1/3 Ni (s) → 1/3 Al_3Ni (s)	−68 [38]
		Al (s) + 1/2 Cu (s) → 1/2 Al_2Cu (s)	−19 [18,39]
Eutectic melting	~930 K [36]	Al (s) + Al_9Co_2 (s) → Al (l) + Al_9Co_2 (s)	+11 [40]
	~910 K [16]	Al (s) + Al_3Ni (s) → Al (l) + Al_3Ni (s)	
	~840 K [20]	Al (s) + Al_2Cu (l) → Al (l) + Al_2Cu (l)	
Al melt	933 K	Al (s) → Al (l)	
Other reactions		Cu + xCo → $CuCo_x$	0–2 [41]
		Cu + xNi → $CuNi_x$	0–1.2 [41,42]
		Ni + xCo → $NiCo_x$	0–1.2 [43]

3.4. *In-situ TEM and EDS*

Fig. 4 presents *in situ* STEM micrographs of nascent Al and Al@CoNiCu nanoparticles at a heating rate of 10 K·min^{-1} under vacuum (10^{-7} Torr), with additional comparisons to Al@Co, Al@Ni, and Al@Cu at 870 K. At room temperature, the surface of Al@CoNiCu exhibits a more corrugated and textured surface compared to the smoother nascent Al nanoparticles. Upon heating, the nascent Al particles remain unchanged until heated above the melting point of Al (>933 K), at which point the molten Al expands within the alumina shell; in particles smaller than 50 nm, this volume expansion causes shell cracking and Al outflow (Fig. 4 (a), yellow arrow). In contrast, Al@CoNiCu nanoparticles, starting from those smaller than 100 nm, begin to exhibit partial hollowing as early as 770 K, and well below the melting point of pure Al, as highlighted by the yellow arrows in Fig. 4(b). By 870 K, all the Al@CoNiCu nanoparticles in view become hollow, with irregular-shaped Al-containing composites growing outside their original shells. More supplementary TEM images (Fig. S3) confirm that this hollowing is a consistent phenomenon. Compared to Al@Co, Al@Ni, and Al@Cu at 870 K (Fig. 4(c–e)), coalescence of the shell metals is observed in all the cases, forming ~10 nm

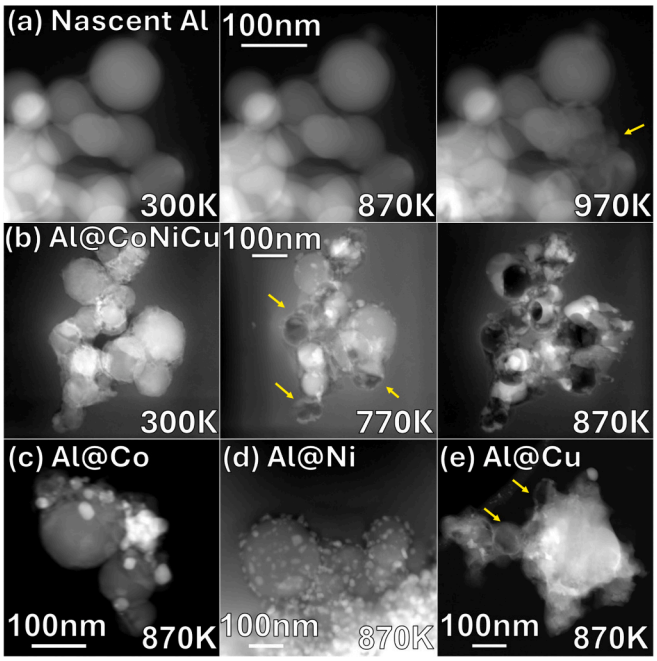

Fig. 4. *In situ* STEM micrograph of (a) nascent Al and (b) Al@CoNiCu under a heating rate of 10 K·min^{-1}, and comparison to (c) Al@Co, (d) Al@Ni, and (e) Al@Cu at 870 K.

Co, Ni, or Cu nanoparticles on the alumina surfaces. Notably, only the Al@Cu particles display partially shell-cracking structures at this temperature, underscoring that the low eutectic point of Al-Cu is one inevitable factor of the early melting and outward flow of Al. Compared to the Al@Cu, the Al outward flow in Al@CoNiCu begins at even lower temperatures (<770 K) and proceeds more extensively, which indicates that the additional exothermic reactions between Al and Ni/Co are important heat contributors to the outward flow of Al in Al@CoNiCu. More STEM-EDS micrographs of Al@Co, Al@Ni, and Al@Cu are compared in supporting Figs. S4–S7.

High-magnification *in situ* STEM-EDS observations in Fig. 5 provide further confirmation of the mechanism. In nascent Al nanoparticles, nanocracks in the alumina shells appear only when heated to around 970 K, driven by volume expansion and surface tension of molten Al. In contrast, the Al@CoNiCu nanoparticles form nanocracks at temperatures below 770 K (Fig. 5(b), yellow arrows), and Al continuously flows outside, mixing with the coated transition metals until the entire nanoparticle becomes nearly hollow. This direct exposure of bare Al promotes rapid alloying or oxidation reactions. In particular, once Al contacts the Ni and Co outside the oxide shell, highly exothermic alloying reactions occur, which further elevate local temperatures and drive additional melting and Al outflow. The formation of the resulting mixed Al/Co/Ni/Cu alloy is shown in Fig. 5(b) in a white dashed-line box. Quantitative EDS analysis reveals that the entropy of mixing is significantly higher for a multi-element system. As shown in Tables 3 and S4, ΔS_{mix} ($=-R(\sum x_i \ln x_i)$) is 1.4 $J{\cdot}mol^{-1}{\cdot}K^{-1}$ for an $Al_{0.962}X_{0.038}$ alloy (considering 30 % Ni/Co formed alloys in Al@Ni and Al@Co), compared to 5.3 $J{\cdot}mol^{-1}{\cdot}K^{-1}$ for an $Al_{0.864}Co_{0.045}Ni_{0.043}Cu_{0.048}$ alloy in Al@CoNiCu, indicating that the mixed alloy formation is thermodynamically favorable. Considering vibrational and other entropy terms

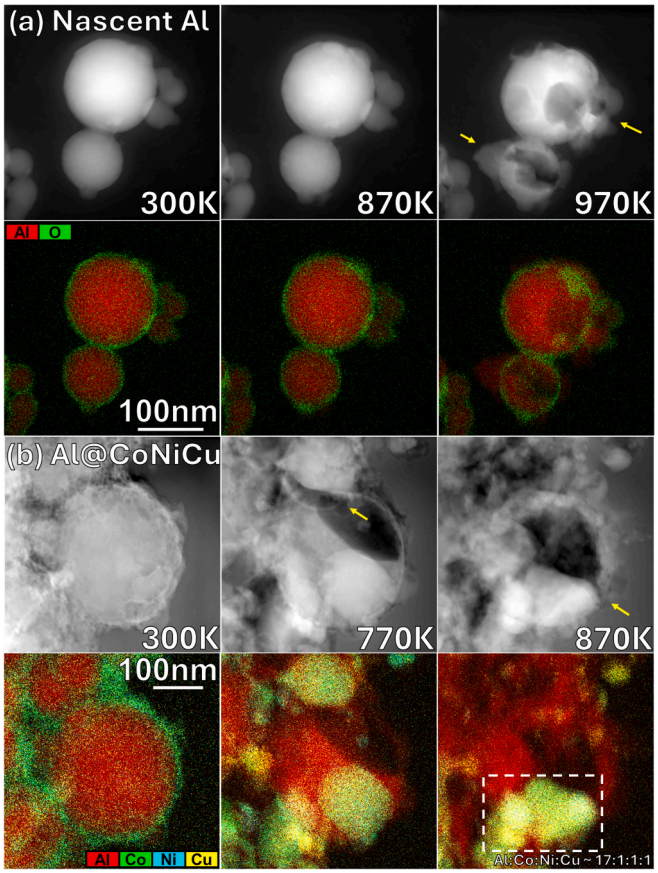

Fig. 5. *In situ* STEM-EDS comparing the heating process of (a) nascent Al and (b) Al@CoNiCu, where yellow arrows highlight the early nanocracks of the Al_2O_3 shell in Al@CoNiCu.

Table 3
Entropy, enthalpy, and Gibbs free energy (per mol Al in sample) during heating of the transition-metal-coated Al nanoparticles based on EDS mapping and DSC results.

Sample	ΔS_{mix} ($J{\cdot}mol^{-1}{\cdot}K^{-1}$)	$T\Delta S_{mix}$ at 870 K ($kJ{\cdot}mol^{-1}$)	ΔH ($kJ{\cdot}mol^{-1}$)	ΔG ($kJ{\cdot}mol^{-1}$)
Al@Co	1.4	1.2	−7.0	−8.2
Al@Ni	1.4	1.2	−8.9	−10.1
Al@Cu	1.7	1.5	−1.6	−3.1
Al@CoNiCu	5.3	4.6	−20.1	−24.7

are often negligible compared to ΔS_{mix} in alloy formations [44], Gibbs free energy of the alloying processes in the synthesized samples can be estimated and listed in Table 3, which indicates that Al@CoNiCu ($\Delta G \sim -24.7$ $kJ{\cdot}mol^{-1}$) has the highest tendency to form mixed alloy. In conclusion, the complete outflow of Al in Al@CoNiCu nanoparticles is mainly driven by the high exothermicity of the Al–Co/Ni reactions (-20.1 $kJ{\cdot}mol^{-1}$) and the favorable entropy of mixing ($T\Delta S_{mix} \sim 4.6$ $kJ{\cdot}mol^{-1}$ at 870 K), which together facilitate early nanocrack formation in the alumina shell and contribute to the significantly reduced ignition temperature observed in these particles.

3.5. Proposed mechanism

In our study, the enhanced ignition behavior of Al@CoNiCu arises from two synergistic diffusion-alloying processes that work together to lower the ignition temperature. First, when Cu is present as a coating (as in both Al@CoNiCu and Al@Cu), the native alumina shell (8-nm thickness) normally acts as a diffusion barrier at room temperature. However, its nanoscale thickness and inherent defects (such as grain boundaries, vacancies, and fragmented regions from sonication as reported by Xu et al. [23–25,45]) may enable rapid, "fast-path" Cu diffusion at elevated temperatures [21,46]. Such defect-assisted migration, facilitated by a relatively low activation energy (~61 kJ/mol) [24], would allow Cu to penetrate the ~8 nm alumina layer and reach the underlying Al core below 800 K. Once localized Cu-Al contact is established, a thin Al_2Cu intermetallic layer nucleates; although its formation is only mildly exothermic, it lowers the local melting point to ~840 K [20,23,24]. In contrast, when Al is coated with Ni or Co (as in Al@Ni and Al@Co), the primary process involves outward diffusion of Al (or inward migration of Ni/Co) through the alumina shell to forming intermetallics (e.g., Al_3Ni and Al_9Co_2). These alloying reactions release a substantial amount of heat, but the eutectic melting of Al-Ni and Al-Co remains close to the melting point of nascent Al at 933 K [16,36].

As illustrated in Fig. 6, the unique behavior of Al@CoNiCu stems from its combination of both mechanisms: the rapid, defect-assisted inward diffusion of Cu leads to the fast formation of Al_2Cu, which in turn lowers the local melting point to ~840 K and triggers localized melting. The ensuing volumetric expansion of molten Al exerts stress that cracks the alumina shell, allowing the outflow of the molten Al to come into direct contact with the surrounding Ni and Co, forming mixed alloys and providing additional heat accelerating further diffusion. This self-reinforcing process is driven by both the high enthalpy of intermetallic reactions and the favorable entropy gain from multi-element mixing disorders.

In summary, while Al@Cu exhibits only weak signals of early Al_2Cu formation and Al@Ni/Al@Co systems solely release heat via gradual outward Al diffusion, the Al@CoNiCu particles combine these synergistic effects into a dual mechanism: rapid Cu diffusion inducing early eutectic melting and significant heat release from subsequent Al–Ni/Al–Co reactions, which leads to rapid volume expansion, early cracking of the alumina shell, and effective Al outward-flow, ultimately resulting in a dramatically reduced ignition temperature.

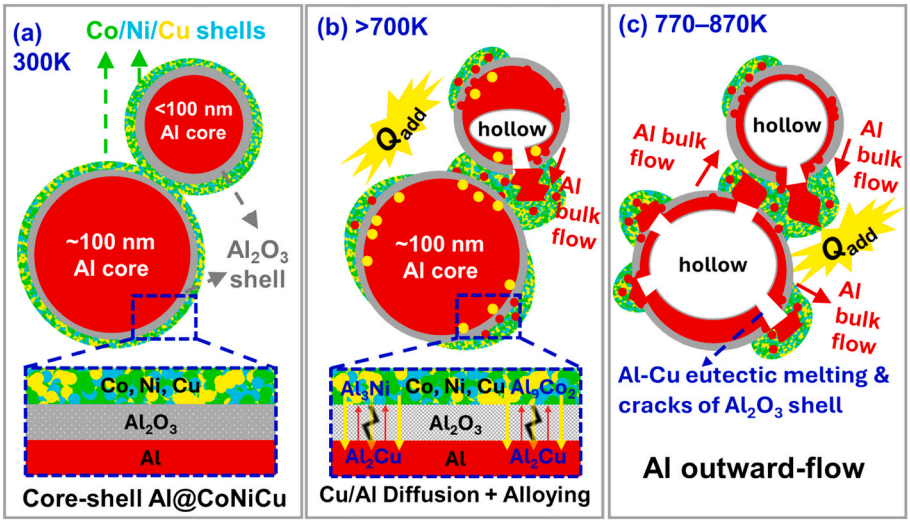

Fig. 6. Illustration on the heating process of Al@CoNiCu at (a) 300 K, (b) 700 K, and (c) 770–870 K.

4. Conclusions

Various transition metals were coated on Al nanoparticles using a one-pot method. The synthesized nanoparticles have lower ignition temperatures compared to nascent Al (ignition temperature from low to high: Al@CoNiCu < Al@Co ≈ Al@Ni < Al@Cu < Al). TGA-DSC analysis reveals that Al@Co and Al@Ni undergo highly exothermic alloying reactions between Al with Co/ Ni, while Al@Cu benefits from the low eutectic melting point of the Al-Cu system. Notably, the hybrid Al@CoNiCu nanoparticles combine the rapid, defect-assisted diffusion of Cu, which triggers the early formation of Al_2Cu and lowers the local eutectic melting point, with the strongly exothermic reactions of Al with Ni and Co. This synergistic mechanism induces early nanocrack formation and outward flow of molten Al at temperatures below 870 K, resulting in markedly lower ignition temperature. By tuning the coating elements, the ignition temperature can be effectively modulated. Moreover, since the native alumina shell is preserved during synthesis, the coated nanoparticles retain better structural integrity than previous methods using displacement reactions, expanding their potential applications.

CRediT authorship contribution statement

Lei Yang: Formal analysis, Data curation, Writing – original draft. **Yuxin Zhou:** Formal analysis, Data curation, Writing – review & editing. **Mahbub Chowdhury:** Data curation. **Yuan Qin:** Data curation. **Matthew M. Dickson:** Resources, Data curation. **Michael R. Zachariah:** Supervision, Resources, Project administration, Methodology, Investigation, Funding acquisition, Conceptualization, Writing – review & editing.

Declaration of competing interest

The authors declare no conflict of interest.

Acknowledgments

This work was supported by the DTRA-MSEE URA and the ONR.

Appendix A. Supplementary data

Supplementary data to this article can be found online at https://doi.org/10.1016/j.cej.2025.164794.

Data availability

Data will be made available on request.

References

[1] D. Sundaram, V. Yang, R.A. Yetter, Metal-based nanoenergetic materials: synthesis, properties, and applications, Prog. Energy Combust. Sci. 61 (2017) 293–365, https://doi.org/10.1016/j.pecs.2017.02.002.
[2] M. Comet, C. Martin, F. Schnell, D. Spitzer, Nanothermites: a short review. factsheet for experimenters, present and future challenges, Propellants Explos. Pyrotech. 44 (2019) 18–36, https://doi.org/10.1002/prep.201800095.
[3] B. Wagner, P. Ghildiyal, P. Biswas, M. Chowdhury, M.R. Zachariah, L. Mangolini, In-flight synthesis of core-shell Mg/Si-SiO_x particles with greatly reduced ignition temperature, Adv. Funct. Mater. 33 (2023) 2212805, https://doi.org/10.1002/adfm.202212805.
[4] R.A. Yetter, G.A. Risha, S.F. Son, Metal particle combustion and nanotechnology, Proc. Combust. Inst. 32 (2009) 1819–1838, https://doi.org/10.1016/j.proci.2008.08.013.
[5] S.H. Kim, M.R. Zachariah, Enhancing the rate of energy release from nanoenergetic materials by electrostatically enhanced assembly, Adv. Mater. 16 (2004) 1821–1825, https://doi.org/10.1002/adma.200306436.
[6] E.L. Dreizin, Metal-based reactive nanomaterials, Prog. Energy Combust. Sci. 35 (2009) 141–167, https://doi.org/10.1016/j.pecs.2008.09.001.
[7] P. Chakraborty, M.R. Zachariah, Do nanoenergetic particles remain nano-sized during combustion? Combust. Flame 161 (2014) 1408–1416, https://doi.org/10.1016/j.combustflame.2013.10.017.
[8] N. Zohari, M.H. Keshavarz, S.A. Seyedsadjadi, The advantages and shortcomings of using nano-sized energetic materials, Cent. Eur. J. Energ. Mater. 10 (2013) 135–147.
[9] K.T. Sullivan, N.W. Piekiel, C. Wu, S. Chowdhury, S.T. Kelly, T.C. Hufnagel, K. Fezzaa, M.R. Zachariah, Reactive sintering: an important component in the combustion of nanocomposite thermites, Combust. Flame 159 (2012) 2–15, https://doi.org/10.1016/j.combustflame.2011.07.015.
[10] S. Chowdhury, K. Sullivan, N. Piekiel, L. Zhou, M.R. Zachariah, Diffusive vs explosive reaction at the nanoscale, J. Phys. Chem. C 114 (2010) 9191–9195, https://doi.org/10.1021/jp906613p.
[11] D.S. Sundaram, P. Puri, V. Yang, A general theory of ignition and combustion of nano- and micron-sized aluminum particles, Combust. Flame 169 (2016) 94–109, https://doi.org/10.1016/j.combustflame.2016.04.005.
[12] J. Zhang, F. Zhao, H. Li, Z. Yuan, M. Zhang, Y. Yang, Q. Pei, Y. Wang, X. Chen, Z. Qin, Improving ignition and combustion performance of Al@Ni in CMDB propellants: effect of nickel coating, Chem. Eng. J. 456 (2023) 141010, https://doi.org/10.1016/j.cej.2022.141010.
[13] C. Wang, X. Zou, S. Yin, J. Wang, H. Li, Y. Liu, N. Wang, B. Shi, Improvement of ignition and combustion performance of micro-aluminum particles by double-shell nickel-phosphorus alloy coating, Chem. Eng. J. 433 (2022) 133585, https://doi.org/10.1016/j.cej.2021.133585.
[14] Z. Cheng, X. Chu, J. Yin, B. Dai, W. Zhao, Y. Jiang, J. Xu, H. Zhong, P. Zhao, L. Zhang, Formation of composite fuels by coating aluminum powder with a cobalt nanocatalyst: enhanced heat release and catalytic performance, Chem. Eng. J. 385 (2020) 123859, https://doi.org/10.1016/j.cej.2019.123859.
[15] R. Ali, F. Ali, A. Zahoor, R.N. Shahid, N.U.H. Tariq, G. Ali, S. Ullah, A. Shah, H. B. Awais, Preparation and oxidation of aluminum powders with surface alumina replaced by iron coating, J. Energ. Mater. 40 (2022) 243–257, https://doi.org/10.1080/07370652.2020.1859647.

[16] H. Okamoto, Al-Ni (aluminum-nickel), J. Phase Equilib. Diffus. 25 (2004) 394, https://doi.org/10.1007/s11669-004-0163-0.
[17] H. Okamoto, Al-Co (aluminum-cobalt), J. Phase Equilibria 17 (1996) 367, https://doi.org/10.1007/BF02665567.
[18] J.L. Murray, The aluminium-copper system, Int. Met. Rev. 30 (1985) 211–234, https://doi.org/10.1179/imtr.1985.30.1.211.
[19] O. Zobac, A. Kroupa, A. Zemanova, K.W. Richter, Experimental description of the Al-Cu binary phase diagram, Metall. Mater. Trans. A 50 (2019) 3805–3815, https://doi.org/10.1007/s11661-019-05286-x.
[20] C. Zhou, L. Jiang, Z. Gu, C. Wang, L. He, L. Huang, Z. Li, K. Li, Flexible core-shell structured Al-Cu alloy phase change materials for heat management, Chem. Eng. J. 471 (2023) 144610, https://doi.org/10.1016/j.cej.2023.144610.
[21] R.H. Doremus, Diffusion in alumina, J. Appl. Phys. 100 (2006) 101301, https://doi.org/10.1063/1.2393012.
[22] F. Moya, E.G. Moya, D. Juvé, D. Tréheux, C. Grattepain, M. Aucouturier, SIMS study of copper diffusion into bulk alumina, Scr. Metall. 28 (1993) 343–348, https://doi.org/10.1016/0956-716X(93)90439-Y.
[23] H. Xu, I. Qin, H. Clauberg, B. Chylak, V.L. Acoff, New observation of nanoscale interfacial evolution in micro Cu–Al wire bonds by in-situ high resolution TEM study, Scr. Mater. 115 (2016) 1–5, https://doi.org/10.1016/j.scriptamat.2015.12.025.
[24] H. Xu, C. Liu, V.V. Silberschmidt, S.S. Pramana, T.J. White, Z. Chen, V.L. Acoff, Behavior of aluminum oxide, intermetallics and voids in Cu–Al wire bonds, Acta Mater. 59 (2011) 5661–5673, https://doi.org/10.1016/j.actamat.2011.05.041.
[25] H. Xu, C. Liu, V.V. Silberschmidt, Z. Chen, V.L. Acoff, Effect of ultrasonic energy on nanoscale interfacial structure in copper wire bonding on aluminium pads, J. Phys. D. Appl. Phys. 44 (2011) 145301, https://doi.org/10.1088/0022-3727/44/14/145301.
[26] B.J. Henz, T. Hawa, M.R. Zachariah, On the role of built-in electric fields on the ignition of oxide coated nanoaluminum: ion mobility versus Fickian diffusion, J. Appl. Phys. 107 (2010) 024901, https://doi.org/10.1063/1.3247579.
[27] V.I. Levitas, B.W. Asay, S.F. Son, M. Pantoya, Melt dispersion mechanism for fast reaction of nanothermites, Appl. Phys. Lett. 89 (2006) 071909, https://doi.org/10.1063/1.2335362.
[28] L. Zhou, N. Piekiel, S. Chowdhury, M.R. Zachariah, T-jump/time-of-flight mass spectrometry for time-resolved analysis of energetic materials, Rapid Commun. Mass Spectrom. 23 (2009) 194–202, https://doi.org/10.1002/rcm.3815.
[29] L. Zhou, N. Piekiel, S. Chowdhury, M.R. Zachariah, Time-resolved mass spectrometry of the exothermic reaction between nanoaluminum and metal oxides: the role of oxygen release, J. Phys. Chem. C 114 (2010) 14269–14275, https://doi.org/10.1021/jp101146a.
[30] P. Ghildiyal, X. Ke, P. Biswas, G. Nava, J. Schwan, F. Xu, D.J. Kline, H. Wang, L. Mangolini, M.R. Zachariah, Silicon nanoparticles for the reactivity and energetic density enhancement of energetic-biocidal mesoparticle composites, ACS Appl. Mater. Interfaces 13 (2020) 458–467, https://doi.org/10.1021/acsami.0c17159.
[31] Y. Jiang, H. Wang, J. Baek, D. Ka, A.H. Huynh, Y. Wang, M.R. Zachariah, X. Zheng, Perfluoroalkyl-functionalized graphene oxide as a multifunctional additive for promoting the energetic performance of aluminum, ACS Nano 16 (2022) 14658–14665, https://doi.org/10.1021/acsnano.2c05271.
[32] H. Wang, Y. Jiang, Y. Wang, J. Baek, X. Zheng, M.R. Zachariah, Enhanced energy delivery of direct-write fabricated reactive materials with energetic graphene oxide, Combust. Flame 260 (2024) 113095, https://doi.org/10.1016/j.combustflame.2023.113095.
[33] Y. Jiang, Y. Wang, J. Baek, H. Wang, J.L. Gottfried, C.-C. Wu, X. Shi, M. R. Zachariah, X. Zheng, Ignition and combustion of perfluoroalkyl-functionalized aluminum nanoparticles and nanothermite, Combust. Flame 242 (2022) 112170, https://doi.org/10.1016/j.combustflame.2022.112170.
[34] G. Jian, N.W. Piekiel, M.R. Zachariah, Time-resolved mass spectrometry of nano-Al and nano-Al/CuO thermite under rapid heating: a mechanistic study, J. Phys. Chem. C 116 (2012) 26881–26887, https://doi.org/10.1021/jp306717m.
[35] A.J. McAlister, The Al-Co (aluminum-cobalt) system, Bull. Alloy Phase Diagr. 10 (1989) 646–650, https://doi.org/10.1007/BF02877635.
[36] A.K. Sfikas, S. Gonzalez, A.G. Lekatou, S. Kamnis, A.E. Karantzalis, A critical review on Al-Co alloys: fabrication routes, microstructural evolution and properties, Metals 12 (2022) 1092, https://doi.org/10.3390/met12071092.
[37] A. Jain, S.P. Ong, G. Hautier, W. Chen, W.D. Richards, S. Dacek, S. Cholia, D. Gunter, D. Skinner, G. Ceder, K.A. Persson, Commentary: the materials project: a materials genome approach to accelerating materials innovation, APL Mater. 1 (2013) 011002, https://doi.org/10.1063/1.4812323.
[38] F.Z. Chrifi-Alaoui, M. Nassik, K. Mahdouk, J.C. Gachon, Enthalpies of formation of the Al–Ni intermetallic compounds, J. Alloys Compd. 364 (2004) 121–126, https://doi.org/10.1016/S0925-8388(03)00493-6.
[39] C. Wolverton, V. Ozoliņš, Entropically favored ordering: the metallurgy of Al_2Cu revisited, Phys. Rev. Lett. 86 (2001) 5518–5521, https://doi.org/10.1103/PhysRevLett.86.5518.
[40] P.J. Linstrom, W.G. Mallard, The NIST chemistry webbook: a chemical data resource on the internet, J. Chem. Eng. Data 46 (2001) 1059–1063, https://doi.org/10.1021/je000236i.
[41] I.V. Nikolaenko, M.A. Turchanin, Enthalpies of formation of liquid binary (copper + iron, cobalt, and nickel) alloys, Metall. Mater. Trans. B Process Metall. Mater. Process. Sci. 28 (1997) 1119–1130, https://doi.org/10.1007/s11663-997-0068-5.
[42] V.P. Glibin, B.V. Kuznetsov, T.N. Vorobyova, Investigation of the thermodynamic properties of Cu–Ni alloys obtained by electrodeposition or by casting, J. Alloys Compd. 386 (2005) 139–143, https://doi.org/10.1016/j.jallcom.2004.05.052.
[43] L.P. Tan, S.P. Padhy, Z. Tsakadze, V. Chaudhary, R.V. Ramanujan, Accelerated property evaluation of Ni-Co materials libraries produced by multiple processing techniques, J. Mater. Res. Technol. 20 (2022) 4186–4196, https://doi.org/10.1016/j.jmrt.2022.08.152.
[44] E.P. George, D. Raabe, R.O. Ritchie, High-entropy alloys, Nat. Rev. Mater. 4 (2019) 515–534, https://doi.org/10.1038/s41578-019-0121-4.
[45] H. Xu, C. Liu, V.V. Silberschmidt, S.S. Pramana, T.J. White, Z. Chen, A re-examination of the mechanism of thermosonic copper ball bonding on aluminium metallization pads, Scr. Mater. 61 (2009) 165–168, https://doi.org/10.1016/j.scriptamat.2009.03.034.
[46] J. Pelleg, Diffusion in alumina single crystals, in: J. Pelleg (Ed.), Diffusion in Ceramics, Springer International Publishing, Cham, 2016, pp. 113–177, https://doi.org/10.1007/978-3-319-18437-1_11.